Differential ZTD estimation based on high spatial resolution NWP data for the Nordic countries

Jan Erik Håkegård, Nadezda Sokolova, Aiden Morrison
SINTEF Digital, Trondheim, Norway
Email: {jan.e.hakegard,nadia.sokolova,aiden.morrison}@sintef.no

***Abstract*—This paper contains results from a study where Numerical Weather Product (NWP) data provided by Norway MET are used to estimate the differential zenith tropospheric delay (dZTD) for an area covering Scandinavia, Finland and the Baltic countries. The NWP data have a high spatial resolution of 2.5×2.5 km, and the estimated dZTD for the grid positions allow for calculation of the tropospheric gradient on short baselines. The results give an indication of how large dZTD values that can be observed for baselines up to 20 km, and where the largest events are located within the coverage area. The motivation for this investigation is to better understand the characteristics of this phenomena and how it might impact high precision and/or high integrity GNSS-based navigation systems in these regions.**

I. Introduction

The tropospheric delay constitutes an important error source for GNSS systems as the signals are both delayed and refracted through the troposphere. While the tropospheric delay phenomena is well understood, accurate modelling of its spatial variation during anomalous tropospheric events and the impact of any unmodelled residuals remains a challenge. Under nominal conditions, the majority of the tropospheric delay can be eliminated by a tropospheric model such as [1] or others, and/or through differential processing. However, during heavy rainfall or other severe weather conditions, tropospheric anomalies may occur causing high spatial variation [2] [3] of the tropospheric delay that cannot be easily mitigated, resulting in residual errors that can affect system accuracy and integrity performance. The focus of this paper is on characterization of the tropospheric delay spatial decorrelation using high resolution numerical weather model data.

The effects of the troposphere on GNSS signals can be exploited to obtain information about the state of the troposphere, and in particular the distribution of water vapor. This is currently a well established field of research and operation referred to as GNSS meteorology [4]. The relationship between GNSS measurements and tropospheric conditions is exploited in other ways as well. GNSS zenith delay estimations are e.g. used for Synthetic Aperture Radar Interferometry (InSAR) tropospheric corrections (see [5] and references therein).

Numerical Weather Products (NWPs) are issued by meteorological organisations such as the ECMWF for Europe and MET Norway for Norway and the surrounding areas. These products contain prognoses of tropospheric parameters such as pressure, temperature and humidity at a number of vertical layers of the troposphere. These parameters can be used to estimate the zenith tropospheric delay (ZTD). The ZTD can be written as the sum of the hydrostatic and wet components, denoted ZHD and ZWD, respectively.

In this study we estimate the differential ZTD (dZTD) from NWP data provided by MET Norway. The resolution of the NWP data is 2.5×2.5 km. The dZTD is calculated as the difference between ZTD values for baselines up to 20 km. The dZTD is related to the tropospheric gradient, and may together with ZHD and ZWD estimates be used to estimate the tropospheric delay based on NWP data.

There exist open data sources for zenith tropospheric delays and gradients, also based on NWP data. The Vienna Mapping Function (VMF) open access data [6] contains ZHT and ZWD data as well as wet north and wet east gradients globally for a grid of resolution $1^\circ \times 1^\circ$. The resolution in latitude is then about 111 km, and in longitude between 30 km and 70 km for latitudes in the range $50^\circ - 70^\circ$N. These data can be used to verify the ZHD and ZWD values estimated from the MET Norway NWP data. The resolution of the VMF data is however too coarse to be used to estimate the differential zenith delays with baselines lower than 20 km, as is done in our study.

In the following sections, the NWP data are briefly described and the model to estimate tropospheric delays from NWP data reviewed. Then, analysis results from one year of NWP data are provided. Results from the analysis are then discussed, before some conclusions are drawn.

II. Model description

A. Data sources

MET Norway provides three NWP products[1]. The MetCoOp Ensemble Prediction System (MEPS) provides 30 ensemble members every six hours with lead times up to 61 hours for a spatial grid of 2.5 km resolution and 61 vertical layers. Arome-Arctic provides one single run up to 66 hour lead time also for a spatial grid of 2.5 km resolution and 61 vertical layers. Finally, post processed products only including surface parameters are provided. Fig. 1 shows the coverage areas of the three products. The green line shows to the MEPS coverage area, the blue line the Arome-Arctic coverage area, and the red line the post processed products coverage area.

This work is supported by the Norwegian Research Council project "Navigation System Integrity Assurance for Safety-Critical Autonomous Operations (NSIA)" (project number 305051).

[1] https://thredds.met.no/thredds/metno.html

This is the author accepted version of an article published in
2022 International Conference on Localization and GNSS (ICL-GNSS)
https://doi.org/10.1109/ICL-GNSS54081.2022.9797016

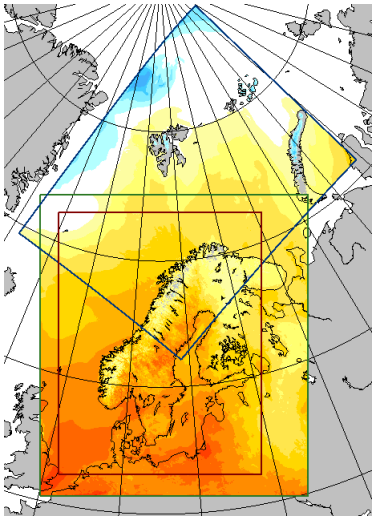

Fig. 1: Coverage area for the NWP products. Blue square: Arome Arctic, green square: MEPS, red square: post processed products (source: MET Norway).

To estimate the tropospheric delay, a 3D model is used. Hence, only the MEPS data and the Arome Arctic data are considered. Both data sets contain the parameters required to estimate the tropospheric delay. In this study, the MEPS data set is selected as it covers the entire Norwegian mainland and surrounding areas. In addition to providing data files with 30 ensemble members, useful for assessing probabilities, it also provides files containing the ensemble member that on average best coincide with observed weather. These are the files used in this study.

B. Relation between NWP data and ZTD

t	time
lat	latitude
lon	longitude
ap	vertical hybrid model
b	vertical hybrid model
ps [Pa]	surface air pressure
θ_0 $[m^2/s^2]$	surface geopotential
q [kg/kg]	model level specific humidity
T [K]	model level air temperature

TABLE I: List of meteorological parameters

In this section, the equations used to derive the tropospheric delay based on NWP data are reviewed. The parameters used as input are listed in Table I. The temporal resolution is 3 hours. Only the forecast with the shortest lead time is considered in this study, as it can be assumed to be the most accurate one. The horizontal grid of longitude, latitude positions has size 739×949.

The ZTD is found by integrating along the vertical model

$$ZTD = 10^{-6} \sum_{k=1}^{L} d(k) N(k) \tag{1}$$

where $d(k)$ is the thickness of vertical layer k, $N(k)$ is the refractivity of level k, and L is the number of vertical layers. Hence, to estimate the ZTD, the thickness of the layers and the refractivity of the layers must be estimated.

1) Estimation of the thickness of the vertical layers: The height of the vertical model layers $h(k)$ is estimated from the air pressure and temperature of each layer. The procedure is provided by MET Norway and consists of integrating from the ground and up [7]:

$$h(k) = h(k+1) + \frac{R \cdot T(k)}{g} \ln\left(\frac{p(k+1)}{p(k)}\right) \tag{2}$$

where $R = 287.058$ J/kgK, T is the temperature in Kelvin found in the data, and p is the pressure in Pascal. The last level $h(L)$ is the surface height h_s found using the following equation:

$$h_s = \frac{\theta_0}{g} \tag{3}$$

where g is the standard gravity. The surface geopotential θ_0 is provided in the data. The pressure at each model level is not included in the data, but can be estimated using the hybrid model parameters. The air pressure at model level k is given by:

$$p(k) = ap(k) + b(k) \cdot ps \tag{4}$$

The components of the hybrid model $ap(k)$ and $b(k)$ and the surface air pressure ps are all available in the data. When the height of each level is derived, we also have the thickness of each level.

2) Estimation of refractivity index: The refractivity index is defined as [8]:

$$N = N_{dry} + N_{wet} = 77.6\frac{p_d}{T} + 72\frac{e}{T} + 3.75 \cdot 10^5 \frac{e}{T^2} \tag{5}$$

where p_d is the dry air pressure in hPa and e is the water vapor pressure in hPa. In this subsection we omit the model layer parameter k for simplicity. The total atmospheric pressure is the sum of the dry and water vapor pressure:

$$p = p_d + e \tag{6}$$

The temperature is available in the data, and the pressure can be estimated using equation (4). The water vapor pressure can be found from the relative humidity RH and the saturation vapor pressure e_s [9]:

$$e = \frac{1}{100} RH \cdot e_s \tag{7}$$

Several different formulas for estimating the saturation vapor pressure are available in the literature. Here, the widely used Magnus formula is used [9]:

$$e_s \approx 611 e^{\left(\frac{17.67(T-T_0)}{T-29.65}\right)} \tag{8}$$

where e_s is in Pascal. T_0 is the reference temperature (typically 273.15 K).

The relative humidity is defined as the ratio of the actual water vapor pressure e to saturation vapor pressure e_s or as the ratio of the actual water vapor dry mas mixing ratio w to

This is the author accepted version of an article published in
2022 International Conference on Localization and GNSS (ICL-GNSS)
https://doi.org/10.1109/ICL-GNSS54081.2022.9797016

the saturation mixing ratio w_s at the ambient temperature and pressure. The two definitions are related as follows:

$$w = \frac{R_d}{R_v}\frac{e}{p-e}, w_s = \frac{R_d}{R_v}\frac{e_s}{p-e_s} \tag{9}$$

where the specific gas constants for dry air $R_d = 287.058$ J/(kgK) and vapor $R_v = 461.5$ J/(kgK). The two definition are essentially equivalent in the cases where $e < e_s << p$.

The specific humidity can be defined as the mass mixing ratio of water vapor in air, defined as:

$$q = \frac{m_v}{m_d + m_v} = \frac{w}{w+1} \approx w \tag{10}$$

The relative humidity can then finally be estimated as:

$$RH = 100\frac{w}{w_s} = 100\frac{R_v}{R_d}\frac{pq}{e_s} \tag{11}$$

and the saturation vapor pressure as:

$$e = \frac{R_v}{R_d}pq = 1.6077pq \tag{12}$$

The refractivity index then becomes:

$$N = N_{dry} + N_{wet} = 77.6\frac{p_d}{T} + 115.75\frac{pq}{T} + 6.0288 \cdot 10^5\frac{pq}{T^2} \tag{13}$$

Care must be taken to the units, as the pressure p using the MET data is in Pa, while equation (5) takes pressure parameters p_d and e in hPa. Hence, p_d and p in equation (13) are in hPa.

The zenith hydrostatic and wet delays can then be estimated as:

$$ZHD = 77.6 \cdot 10^{-6}\sum_{k=1}^{L} d(k)\frac{p_d(k)}{T(k)} \tag{14}$$

$$ZWD = 10^{-6}\sum_{k=1}^{L} d(k)\left(\frac{115.75}{T(k)} + \frac{6.0288 \cdot 10^5}{T^2(k)}\right)p(k)q(k) \tag{15}$$

C. Differential ZTD

The differential ZTD (dZTD) is calculated as the difference between the estimated ZTD values. dZTD values for baselines up to 20 km are considered of interest. It would be too computationally expensive to calculate all the dZTD values for baselines up to 20 km. Therefore, a grid with resolution 20×20 km is generated, and the maximum and minimum ZTD values within each 20×20 km pixel are found and stored together with the corresponding baseline. The coverage area consists of 69×87 pixels.

Only horizontal dZTD is considered. Due to the varying surface height, dZTD values are calculated for seven heights above sea level: 10m, 200m, 400m, 600m, 800m, 1000m and 1600m. Only the results from the height providing the highest dZTD value for each pixel are retained.

D. Relation between differential ZTD and tropospheric gradient

The slant tropospheric delay (STD) of GNSS signals can be expressed as:

$$\begin{aligned} STD(el, az) = m_h(el)ZHD + m_w(el)ZWD \\ + m_g\left(\cos(az)N + \sin(az)E\right), \end{aligned} \tag{16}$$

where az and el are the azimuth and elevation angles, N and E are the north and east gradient components, and m_h, m_w and m_g are mapping functions. The gradient represents the first-order asymmetry of the tropospheric delay. Several mapping functions exist. Most commonly used are CfA-2.2, Ifadis, mapping temperature test (MTT), Neill's mapping function (NMF), Global mapping function (GMF), and Vienna mapping function (VMF1) [10].

The gradient components can be split into hydrostatic and wet components in the same way as the ZTD. For the wet components, the following is approximately true [11]:

$$\begin{aligned} E_w \approx C\frac{\partial ZWD}{\partial x} = \frac{C}{R}\frac{\partial ZWD}{\partial \lambda}\frac{1}{\cos\phi} \\ N_w \approx C\frac{\partial ZWD}{\partial y} = \frac{C}{R}\frac{\partial ZWD}{\partial \phi}, \end{aligned} \tag{17}$$

where λ and ϕ denote the station latitude and longitude and R is the Earth's radius. C is related to the scale height of the wet refractivity gradient and is set to 4 km in [11].

In this study we use a slightly different approach. The gradient G is approximated as the difference between ZWD values divided by the baseline:

$$G \approx \frac{ZWD(x_1, y_1) - ZWD(x_2, y_2)}{d((x_1, y_1), (x_2, y_2))}, \tag{18}$$

where $ZWD(x_1, y_1)$ and $ZWD(x_2, y_2)$ are the maximum and minimum ZWD estimates within the 20×20 km pixel, and $d((x_1, y_1), (x_2, y_2))$ is the distance. As the goal has not been to estimate the STD using (16), we have not split the gradient into north and east components. A scale height C is not set for the same reason.

III. Results

A. MEPS coverage area

dZTD values are calculated based on files from MET issued each 3 hours during 2021, hence for 2920 epochs. Fig. 2 shows the maximum estimated dZTD in each epoch for the MEPS coverage area shown in Fig. 1. Hence, the curve does not correspond to one location, but to the maximum estimated dZTD value for the entire coverage area for each epoch. The curve clearly shows that the highest dZTD values are observed during the summer months, from mid May to the end of August.

Table II shows the five highest estimated dZTD values during 2021, including the time and the corresponding baseline. The highest estimated dZTD event occurred 14 July just north of Gothenburg and the estimated dZTD was 18.1 cm with baseline 17.7 km, corresponding to a gradient of 10.2 mm/km using (18).

This is the author accepted version of an article published in
2022 International Conference on Localization and GNSS (ICL-GNSS)
https://doi.org/10.1109/ICL-GNSS54081.2022.9797016

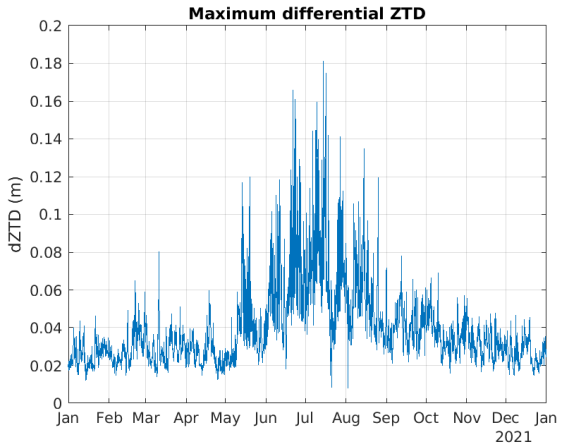

Fig. 2: Maximum dZTD values as function of time.

	Time	dZTD (m)	Baseline (km)
1	14-Jul-2021 12:00:00	0.181	17.7
2	16-Jul-2021 12:00:00	0.175	14.6
3	21-Jun-2021 15:00:00	0.166	10.6
4	23-Jun-2021 00:00:00	0.161	12.5
5	09-Jul-2021 12:00:00	0.159	10.0

TABLE II: List of dZTD events

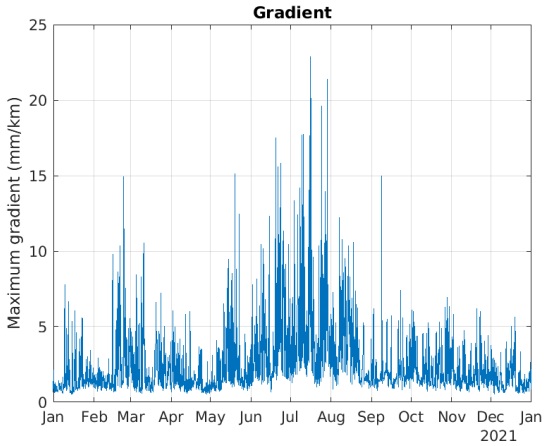

Fig. 3: Maximum gradient as function of time.

Fig. 3 shows the horizontal gradients in mm/km for the maximum dZTD events, again using (18). The steepest gradient of 22.8 mm/km is estimated 16 July, with dZTD of 11.4 cm and a baseline of 5 km. It should be noted that these gradients are calculated for the maximum dZTD value per pixel. It is likely that there exist larger gradients with shorter baselines.

Fig. 4 shows where the 50 strongest dZTD events occur. Almost all of them are located in the eastern part of the coverage area, i.e., in Finland and the Baltic countries. Only five are located in Sweden, one in Norway, and one in Skagerrak.

It was surprising that almost all events are in the eastern parts of the coverage area, and it was therefore looked further

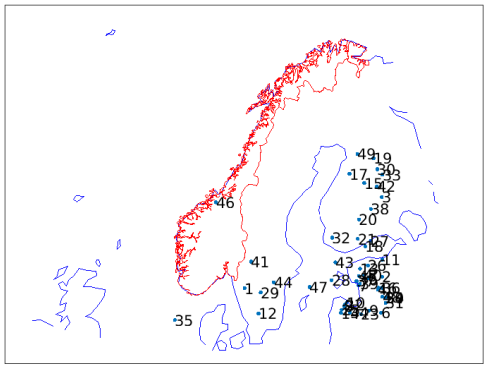

Fig. 4: 50 events with maximum dZTD value.

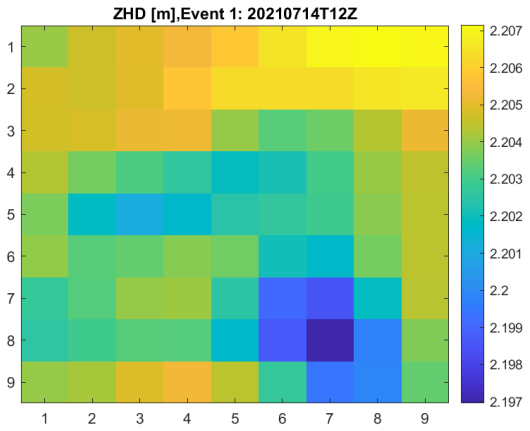

Fig. 5: ZHD values for 20×20 km pixel with highest dZTD.

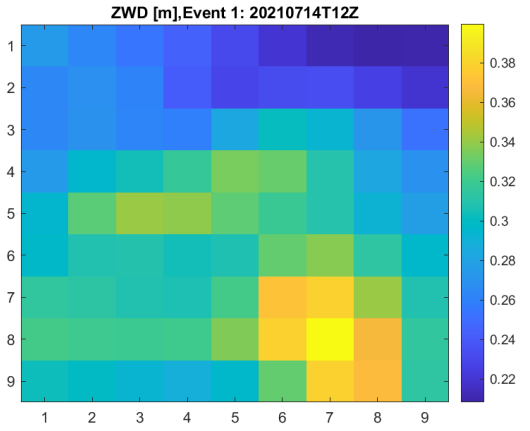

Fig. 6: ZWD values for 20×20 km pixel with highest dZTD.

into. Figs. 5 and 6 show the estimated ZHD and ZWD values for the pixel giving the highest dZTD value. The area covered by the figures is hence 20×20 km, and the resolution is

This is the author accepted version of an article published in
2022 International Conference on Localization and GNSS (ICL-GNSS)
https://doi.org/10.1109/ICL-GNSS54081.2022.9797016

2.5×2.5 km. The figures confirm that it is the ZWD that constitutes the major contribution to the dZTD. Although the magnitude of the ZHD is higher and in the order of 2.2 m, the variations on the ZWD value are significantly higher.

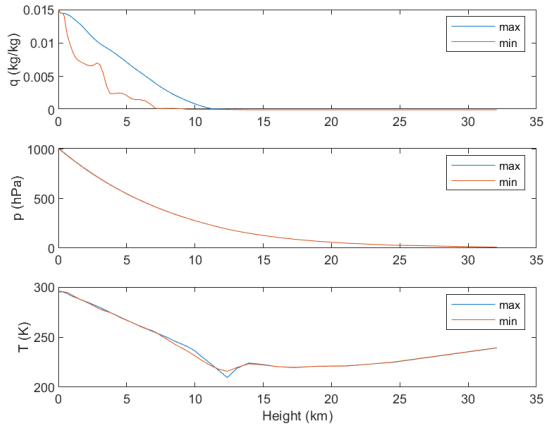

Fig. 7: Specific humidity q, pressure p and temperature T as function of height for the pixel with highest dZTD.

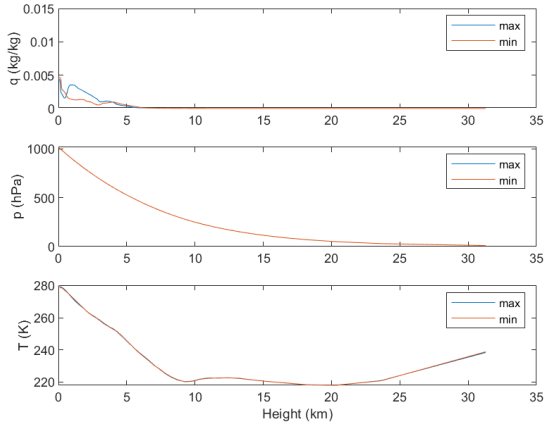

Fig. 8: Specific humidity q, pressure p and temperature T as function of vertical layer for a pixel with typical dZTD.

The ZWD depends on the three model parameters p, q and T, as can be seen from (15). Fig. 7 shows how the three parameters vary with height for the maximum dZTD event. The red and blue curves correspond to the maximum and minimum ZTD value, respectively. As expected, the pressure and temperature is very similar for the two locations, while the specific humidity q is significantly higher for the location with maximum ZTD value. Fig. 8 corresponds to a typical epoch where the dZTD value is in the order of 3 mm and is included for reference. The specific humidity curves for all the largest events show the same behaviour as in Fig. 7, while the curves for arbitrary pixels and epochs show the same behaviour as in Fig. 8. It therefore seems as events with more fluctuations in the specific humidity occur more often in the eastern part of the coverage area than in other parts of the coverage area.

The data shown in this section only include the maximum dZTD values over the entire coverage area at each epoch. It may therefore be the case that there are events with higher dZTD values in Norway that are not included because they are masked by even higher dZTD values at the same time outside Norway. To check this, we consider the data only for the mainland of Norway in the next section.

B. Analysis of data from Norwegian mainland

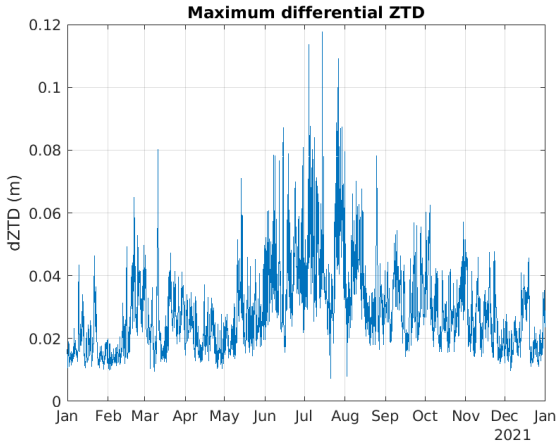

Fig. 9: Estimated dZTD values for Norway

	Time	dZTD (m)	Baseline (km)
1	14-Jul-2021 12:00:00	0.118	13.5
2	04-Jul-2021 12:00:00	0.114	13.5
3	26-Jul-2021 18:00:00	0.109	10.3
4	04-Jul-2021 15:00:00	0.092	20.0
5	26-Jul-2021 15:00:00	0.091	20.7

TABLE III: List of dZTD events in Norway

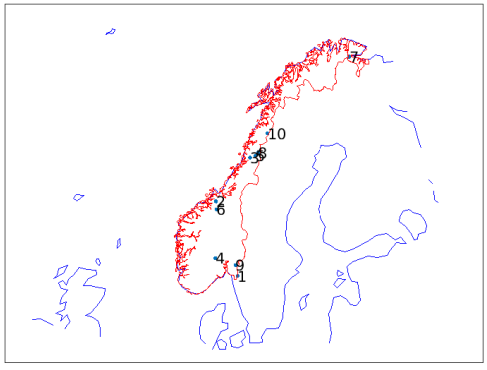

Fig. 10: 10 events with maximum dZTD value in Norway.

Fig. 9 shows the maximum estimated dZTD values for Norway. The highest value occurred 14 July at noon close

This is the author accepted version of an article published in
2022 International Conference on Localization and GNSS (ICL-GNSS)
https://doi.org/10.1109/ICL-GNSS54081.2022.9797016

to Halden. Hence, this is the same event that caused the 18.1 cm event at the same time a few km further to the south in Sweden.

Table III lists the five largest observed dZTD events in Norway. The three largest ones are over 10 cm. Fig. 10 illustrates the geographical distribution of the estimated dZTD values. As can be seen, they are scattered from the southern parts of Norway to Finmark in the north. Events 3 and 5 are in fact part of the same meteorological event, as they are from consecutive epochs and almost co-located. Events 2 and 4 are from consecutive epochs, but are located within different parts of Norway.

IV. Discussions

The high resolution of the MEPS data provides an opportunity to estimate local variations in the tropospheric delay based on NWP data that other sources providing $1^\circ \times 1^\circ$ resolution do not support. The dynamic and in-homogeneous nature of the humidity of the troposphere requires data samples with a high density for the linear expansion of the derivative at a certain point to be reasonably accurate. The high resolution is however a challenge computationally. The methodology used to estimate maximum dZTD values in this study gives an indication of how much the ZTD, and hence ZWD, may vary over distances up to 20 km. It does however not do an exhaustive search, as that would be too time consuming. Dividing the coverage area into 20 km pixels and only considering the maximum and minimum values within a pixel opens the possibility that two locations will exist within 20 km distance, but in different pixels, may provide higher dZTD values. Still, considering the high number of epochs and the large coverage area, it is considered unlikely that considerably higher dZTD values are missed.

Another feature of the method used in this study is that the maximum dZTD value within each pixel is found. This may not coincide with the highest gradient within the pixel, as lower dZTD values with shorter baselines may lead to steeper gradients. The reason for this choice is also to reduce the computational load. A continuation of the work could include to select epochs and locations where large dZTD values are observed, and find the steepest gradients in those data sets.

Studies from other parts of the world report spike events up to 300 mm/km [12]. One reason for this is that convective rain events with higher intensity occur further to the south. Such events tend to be very local and of short duration. Moreover, the NWP data will represent an averaging over both the 2.5×2.5 km spatial area and over the 3 hour time resolution. Measurements may therefore capture very local and short duration events that the NWP data miss. The same effect is observed when comparing NWP data with weather radar data, where the radar data show higher maximum values for rain rates. The NWP data sets contain variability parameters that may be used to statistically interpolate in both the spatial and temporal domains, but these are not used in this study.

The results obtained from this study can be compared to ZWD estimates obtained from a cluster of GNSS receivers. As the NWP data provide predictions of the meteorological parameters, and do not constitute ground truth, there are bound to be differences in the results. Combining GNSS measurements and results from NWP data may however provide an improved estimation of the tropospheric gradients.

V. Conclusions

In this study, a set of NWP data covering the year 2021 is used to find the maximum differential ZTD values for baselines up to 20 km. The data covers the Nordic countries, Finland and the Baltic region. The results show that dZTD values approaching 20 cm can be observed, and gradients of approximately 25 mm/km can be found. Most of the observed events occurred in the eastern parts of the coverage area, though it should be noted that this study relied on only one year of data, so this may not be fully representative.

The high resolution of the NWP data may provide a better approximation of the tropospheric gradient of GNSS signals than using estimates from the GNSS stations alone. The implications of the observed dZTD and gradient values for GNSS navigation users are limited compared to gradients that can be encountered in other regions.

References

[1] J. Saastamoinen, "Contributions to the theory of atmospheric refraction," *Bulletin Geodesique*, vol. 46, pp. 279–298, Sep. 1972. [Online]. Available: https://ui.adsabs.harvard.edu/abs/1972BGeod..46..279S

[2] S. Khanafseh, A. Engeln, B. Pervan, and I. Technology, *Tropospheric Duct Anomaly Threat Model for High Integrity and High Accuracy Navigation*, Nov. 2016, pages: 1616.

[3] J. Huang, F. van Graas, and C. Cohenour, "Characterization of Tropospheric Spatial Decorrelation Errors Over a 5-km Baseline," *NAVIGATION, Journal of the Institute of Navigation*, vol. 55, no. 1, pp. 39–53, Mar. 2008. [Online]. Available: http://www.ion.org/publications/abstract.cfm?jp=j&articleID=102461

[4] G. Guerova, J. Jones, J. Douša, G. Dick, S. de Haan, E. Pottiaux, O. Bock, R. Pacione, G. Elgered, H. Vedel, and M. Bender, "Review of the state of the art and future prospects of the ground-based GNSS meteorology in Europe," *Atmospheric Measurement Techniques*, vol. 9, no. 11, pp. 5385–5406, Nov. 2016, publisher: Copernicus GmbH. [Online]. Available: https://amt.copernicus.org/articles/9/5385/2016/

[5] N. Roukounakis, P. Elias, P. Briole, D. Katsanos, I. Kioutsioukis, A. A. Argiriou, and A. Retalis, "Tropospheric Correction of Sentinel-1 Synthetic Aperture Radar Interferograms Using a High-Resolution Weather Model Validated by GNSS Measurements," *Remote Sensing*, vol. 13, no. 12, p. 2258, Jan. 2021, number: 12 Publisher: Multidisciplinary Digital Publishing Institute. [Online]. Available: https://www.mdpi.com/2072-4292/13/12/2258

[6] "re3data.org: Vmf data server; editing status 2020-12-14; re3data.org - registry of research data repositories." [Online]. Available: https://vmf.geo.tuwien.ac.at/

[7] "Calculating model level height." [Online]. Available: https://github.com/metno/NWPdocs/wiki/Calculating-model-level-height

[8] "RECOMMENDATION ITU-R P.453-14 - The radio refractive index: its formula and refractivity data," p. 24.

[9] M. G. Lawrence, "The Relationship between Relative Humidity and the Dewpoint Temperature in Moist Air: A Simple Conversion and Applications," *Bulletin of the American Meteorological Society*, vol. 86, no. 2, pp. 225–234, Feb. 2005, publisher: American Meteorological Society Section: Bulletin of the American Meteorological Society. [Online]. Available: https://journals.ametsoc.org/view/journals/bams/86/2/bams-86-2-225.xml

This is the author accepted version of an article published in
2022 International Conference on Localization and GNSS (ICL-GNSS)
https://doi.org/10.1109/ICL-GNSS54081.2022.9797016

[10] C. Qiu, X. Wang, Z. Li, S. Zhang, H. Li, J. Zhang, and H. Yuan, "The Performance of Different Mapping Functions and Gradient Models in the Determination of Slant Tropospheric Delay," *Remote Sensing*, vol. 12, no. 1, p. 130, Jan. 2020, number: 1 Publisher: Multidisciplinary Digital Publishing Institute. [Online]. Available: https://www.mdpi.com/2072-4292/12/1/130

[11] F. Zus, J. Douša, M. Kačmařík, P. Václavovic, K. Balidakis, G. Dick, and J. Wickert, "Improving GNSS Zenith Wet Delay Interpolation by Utilizing Tropospheric Gradients: Experiments with a Dense Station Network in Central Europe in the Warm Season," *Remote Sensing*, vol. 11, no. 6, p. 674, Jan. 2019, number: 6 Publisher: Multidisciplinary Digital Publishing Institute. [Online]. Available: https://www.mdpi.com/2072-4292/11/6/674

[12] A. Schüttpelz, F. Beck, S. Saito, D. Weed, and B. Johnson, "Characterization of the tropospheric gradient effects affecting the ionospheric monitoring," *WP/20, ICAO NSP CSG*, Feb. 2015.

This is the author accepted version of an article published in
2022 International Conference on Localization and GNSS (ICL-GNSS)
https://doi.org/10.1109/ICL-GNSS54081.2022.9797016